J Arid Land (2021) 13(2): 189–204
https://doi.org/ 10.1007/s00000-021-0093-1

Science Press Springer-Verlag

Spatial variability and temporal stability of actual evapotranspiration on a hillslope of the Chinese Loess Plateau

ZHANG Yongkun[1], HUANG Mingbin[2*]

[1] State Key Laboratory of Plateau Ecology and Agriculture, Qinghai University, Xining 810016, China;
[2] Institute of Soil and Water Conservation, Northwest Agriculture and Forestry University, Yangling 712100, China

Abstract: Actual evapotranspiration (ET_a) is a key component of water balance. This study aimed to investigate the spatial variability and time stability of ET_a along a hillslope and to analyze the key factors that control the spatiotemporal variability of ET_a. The potential evaporation, surface runoff and 0–480 cm soil water profile were measured along a 243 m long transect on a hillslope of the Loess Plateau during the normal (2015) and wet (2016) water years. ET_a was calculated using water balance equation. Results indicated that increasing precipitation during the wet water year did not alter the spatial pattern of ET_a along the hillslope; time stability analysis showed that a location with high time stability of ET_a could be used to estimate the mean ET_a of the hillslope. Time stability of ET_a was positively correlated with elevation ($P<0.05$), indicating that, on a hillslope in a semi-arid area, elevation was the primary factor influencing the time stability of ET_a.

Keywords: relative difference; water balance; surface runoff; soil texture; semi-arid areas

Citation: ZHANG Yongkun, HUANG Mingbin. 2021. Spatial variability and temporal stability of actual evapotranspiration on a hillslope of the Chinese Loess Plateau. Journal of Arid Land, 13(2): 189–204. https://doi.org/10.1007/s00000-021-0093-1

1 Introduction

Actual evapotranspiration (ET_a) is an important component of water and energy cycle, and it accounts for 95% of water balance in dry ecosystems (Wilcox et al., 2003). Moreover, water-limited environments cover almost half of the Earth's land surface and are expected to increase (Newman et al., 2006). Therefore, understanding the spatiotemporal variations of ET_a is crucial for water resources management efficiency in water-limited regions (Lian and Huang, 2015, 2016).

ET_a is perhaps the most difficult and complicated component of the hydrological cycle because it involves the combined effects of climate, terrain, vegetation, soil and its hydraulic properties (Thomas, 2000; Xu and Singh, 2005; McVicar et al., 2007; Vivoni et al., 2010; Zhao and Zhao, 2014; Li et al., 2017). Many studies have focused on the spatiotemporal variability of ET_a under different environmental conditions (Thomas, 2000; Mo et al., 2004; Gao et al., 2007; McVicar et al., 2007; Vivoni et al., 2010; Gao et al., 2019). For example, Thomas (2000) reported that evapotranspiration in the arid and semi-arid areas of Northwest China decreased to a large extent in all seasons primarily due to variations in wind, relative humidity and maximum temperature. Nicholls et al. (2016) analyzed the effect of vegetation cover on ET_a in the 52-hm^2 Sandhill Fen

*Corresponding author: HUANG Mingbin (E-mail: hmingbin@yahoo.com)
Received 2019-09-09; revised 2020-10-25; accepted 2020-12-22

watershed of Canada, and found that ET_a increased as the peak leaf area index (LAI) increased during the growing season. Mo et al. (2004) simulated annual ET_a over the Lushi basin in the middle reach of the Yellow River of China, and suggested that spatial pattern of annual ET_a was similar to precipitation and LAI patterns. Vivoni et al. (2010) explored soil moisture and evapotranspiration distributions using a distributed hydrologic model in a semi-arid mountain basin, and found hysteresis existed between soil moisture and evapotranspiration due to climate variability.

The above studies on the spatiotemporal variability of ET_a were mainly conducted at the regional or watershed scales. The hillslope is the main unit of measurement in hydrological studies where ET_a measurements are used to derive catchment-level ET_a (Santiago et al., 2000; Ewers et al., 2002). However, systematic studies on the spatiotemporal variability of ET_a at the hillslope scale remain scarce. Carey and Woo (2001) investigated the differences in ET_a on four hillslopes with different vegetation types, and stated that ET_a was mainly limited by the phenology of deciduous forests and shrubs. Because there was only one measurement site for ET_a on each hillslope, spatial variability of ET_a within the hillslope was ignored in the study of Carey and Woo (2001). Mitchell et al. (2012) evaluated the differences in ET_a at different hillslope positions in a mixed-species eucalypt forest, and discovered that ET_a in the upper slope position is 40% lower than that in the middle and lower slope positions. Because the ET_a measurement sites in the study of Mitchell et al. (2012) were located on different hillslopes in the catchment, differences in ET_a between measurement sites was not necessarily due to slope position. However, many environmental factors might cause differences in ET_a along a hillslope (Majidi et al., 2015). And just measuring ET_a at one monitoring site on a hillslope is difficult to understand the spatiotemporal variability of ET_a at the hillslope scale. In this study, a transect line was established on a hillslope with single vegetation type to obtain the ET_a at different positions of the hillslope, so as to understand the spatial variability of ET_a inside the hillslope.

ET_a always presents temporal variability at different positions on the hillslope. A time stability analysis can be performed to investigate the spatial variability and time stability of ET_a at the hillslope scale. In previous studies, this method has been successfully applied to examine the spatiotemporal variability of soil moisture at hillslope and catchment scales. And the most time stable location (MTSL) in the studied field is identified to represent the mean soil moisture of the field (Vachaud et al., 1985; Starr, 2005; Hu et al., 2010; Gao et al., 2011; Gao and Shao, 2012; Jia and Shao, 2013; Hu and Si, 2014; Zhang et al., 2016; Liao et al., 2017). Recently, two indices (soil salinity and soil sulfur content) except for soil moisture have applied time stability analysis to analyze the spatiotemporal variability (Douaik et al., 2006; Piotrowska-Długosz et al., 2017). However, no study has been conducted to investigate the spatiotemporal variability of ET_a by a time stability analysis.

In this study, we assume that time stability analysis can be utilized for investigation of spatiotemporal variability of ET_a at a hillslope scale. The objectives of the present study are: (1) to investigate the spatial variability of water balance components along a hillslope; (2) to explore the spatial variability and time stability of ET_a along the hillslope; and (3) to determine the primary factors controlling the spatiotemporal variability of ET_a on the hillslope.

2 Materials and methods

2.1 Study area

The study was conducted on a hillslope located in Liudaogou Watershed (38°46′–38°51′N, 110°21′–110°23′E) on the Chinese Loess Plateau (Fig. 1). The watershed is characterized by semi-arid continental climate conditions (Peel et al., 2007), with a mean annual air temperature and precipitation of 8.4°C and 437 mm (1980 to 2015), respectively. The annual precipitations in 2015 (435 mm) and 2016 (612 mm) are equal to or 25% higher than the mean annual precipitation (437 mm), thus the years of 2015 and 2016 are termed as normal and wet water years (Zhang et al., 2016). The watershed covers an area of 6.89 km^2 and features a series of deep gullies and large slopes. The dominant soil is Inceptisols with texture of silt loam (Fu et al., 2012). The soil forms in loess parent material. As a result, it has substantial macropores and vertical fractures, leading to good drainage. The annual potential evapotranspiration is approximately 785 mm

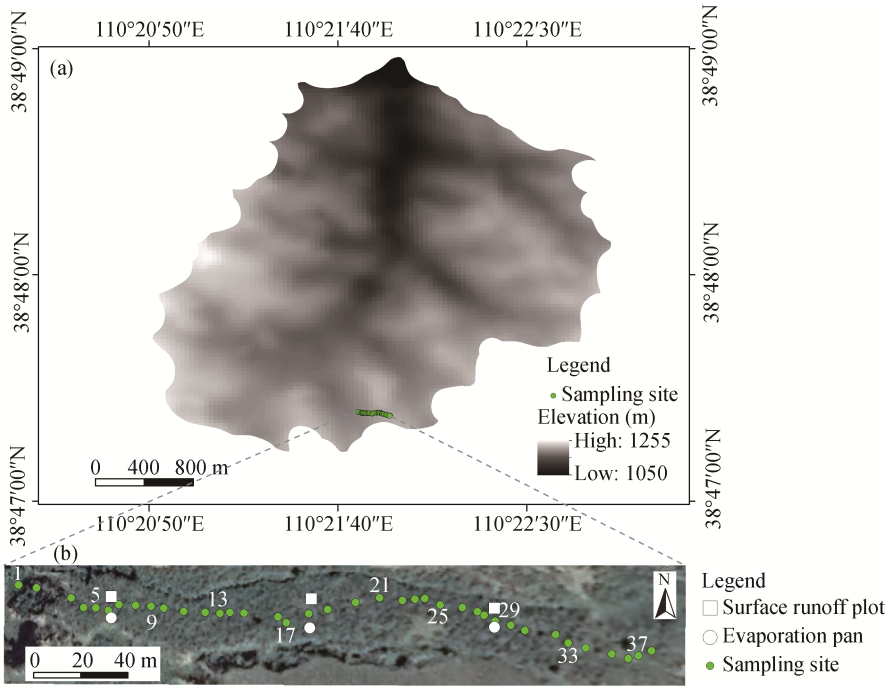

Fig. 1 Sampling sites in (a) Liudaogou watershed and (b) layout of 38 soil water content monitoring locations spaced at 5 m intervals on a hillslope. Surface runoff experimental plots and evaporation pans at the upper (sampling site, 1–13), middle (sampling site, 14–27), and lower (sampling site, 28–38) slope positions.

(Hu and Si, 2014). The elevation ranges from 1094 to 1274 m (Bo et al., 2011). The studied hillslope is approximately 243 m long and 20 m wide and runs from southeast to northwest with mean slope gradient of about 19.8°. The hillslope is mainly vegetated with Korshinsk peashrub (*Caragana korshinskii* Kom). The relevant soil properties, terrain attributes, and vegetation features are provided in Table 1. Three plots were established at the upper, middle and lower slope positions. Each plot was 2 m×5 m with the longest side in the direction of the slope gradient. Five, five and six shrubs (*C. korshinskii*) with similar canopies are successively distributed in the upper, middle and lower plots on the hillslope, respectively. The mean slope gradients of upper, middle and lower slope positions are 27.7°, 22.7° and 12.1°, respectively, as displayed in Table 1.

2.2 Data collection

A transect running down the middle of the hillslope was used for soil water content (SWC) measurements in 40 sampling locations established at approximately 5 m intervals (Fig. 1b). Sampling locations were referred to as locations 1 to 38 from the top to the bottom of the slope because measurements at locations 39 and 40 ceased in 2016. Locations 1 to 13, 14 to 26, and 27 to 38 represented the upper, middle, and lower slope positions, respectively. A 5-m long aluminum neutron probe access tube was installed at each sampling location. Considering that the root system of Korshinsk peashrub was distributed in the 0–500 cm soil profile (Cheng et al., 2009), SWC was measured at 10-cm depth intervals between the depths of 10 and 100 cm and at 20-cm intervals between the depths of 120 and 480 cm. Measurements were made approximately every 12 d during the observation periods (1 May to 26 October 2015 and 15 April to 29 October 2016). Volumetric SWC was measured by a neutron probe (CNC503DR hydro probe; Beijing Super Power Company, China). In the 0–10 and 10–20 cm soil profiles, loss of fast thermal neutrons from the soil usually occurs and requires a separate calibration of the neutron probe for each of the two layers (Bromley et al., 1997). Calibration of the neutron probe was performed with standard methods by measuring the counts at fixed depths in seven 480-cm long access tubes installed in the hillslope along the transect with a wide range of SWCs (soil water contents).

Table 1 Soil properties, topographic attributes, and vegetation features at different slope positions along the hillslope

Property	Soil profile (cm)	Statistical parameter	Slop position		
			Upper	Middle	Lower
ELE (m)		Max	1170	1151	1140
		Min	1152	1141	1131
		Mean±SD	1159±4.72[a]	1146±3.83[b]	1136±3.13[c]
Slope (°)		Max	24.32	16.56	9.21
		Min	34.10	25.43	16.23
		Mean±SD	27.69±2.90[a]	22.69±3.09[b]	12.12±2.07[c]
K_s (cm/h)	0–30	Max	6.20	7.66	6.31
		Min	1.57	1.97	0.89
		Mean±SD	3.00±1.52[a]	3.76±1.78[b]	2.52±1.65[a]
BD (g/cm^3)	0–30	Max	1.61	1.73	1.74
		Min	1.25	1.32	1.13
		Mean±SD	1.39±0.09[a]	1.48±0.1[a]	1.53±0.11[a]
LAI_m (m^2/m^2)		Max	1.86	2.32	2.96
		Min	0.62	0.61	0.55
		Mean±SD	1.13±0.33[a]	1.56±0.22[b]	1.47±0.25[b]
Clay (%)	0–200	Max	16.62	16.26	16.80
		Min	9.42	12.33	5.46
		Mean±SD	13.56±2.24[a]	14.70±1.2[a]	12.97±3.15[a]
Silt (%)	0–200	Max	40.33	41.71	42.44
		Min	26.55	31.58	15.59
		Mean±SD	35.26±4.94[a]	37.20±2.89[a]	31.57±7.28[a]
Sand (%)	0–200	Max	64.02	55.65	78.95
		Min	43.32	42.69	40.76
		Mean±SD	51.19±7.01[a]	48.10±4.00[a]	55.46±10.38[a]

Note: ELE, mean elevation; K_s, saturated hydraulic conductivity; BD, bulk density; LAI_m, maximum leaf area index (measured on 12 August 2015). Upper, middle, and lower slope positions respectively represent the sampling sites 1–13, 14–27, and 28–38. The same lowercase letters within a row indicate no significant difference at $P<0.05$ level.

The standard count was obtained when the probe was immersed in water. The relation between soil moisture counts and standard counts was then calibrated against the volumetric SWC of 200 soil cores extracted from each of the fixed depths and at the same horizontal distance from the access tube measured with standard methods (Gardner et al., 2001).

During the installation of the neutron probe access tubes, disturbed soil samples were collected for soil texture determination. The soil samples were collected at 20-cm depth intervals down to a depth of 200 cm in each neutron probe access tube location. Soil texture was relatively homogeneous throughout the entire soil profile, except for the soil surface during the installation of neutron probe access tubes. Thus, only the soil particle size distribution of the 0–200 cm soil profile was measured. Soil particle size distribution was determined by laser diffraction using Mastersizer 2000 (Malvern Ltd., UK). In addition, at each location, three 40-cm deep soil profile pits were excavated at distances of 50 cm from the tube. Undisturbed soil samples were collected from the pit walls at a depth of 30 cm by using standard pre-weighed 100 ml Kopecky rings. The soil samples were used to determine bulk density (BD) through the gravimetric method (Baker, 1990) and saturated hydraulic conductivity (K_s) through the constant-head method (Libardi et al., 1980). Three replicated samples were collected in each location. The statistics of BD and K_s are listed in Table 1.

LAI was measured with an LAI-2200 canopy analyzer (Li-Cor, Inc., USA). Plots with a size of 2 m×2 m were created and centered on the access tube in each location. From each of these plots, three Korshinsk peashrub plants were selected to determine the LAI in each month of the

monitoring period. Each plant was considered a replicate, and the LAI values of the three plants were utilized to calculate the mean LAI in that SWC monitoring location. The maximum LAI values were measured on 12 August 2015 and 18 August 2016. The mean values of the maximum LAI for the three slope positions are shown in Table 1. The elevation (E) and slope in each location were determined with an RTK-GPS receiver (Trimble 5700, Trimble Inc., USA) and a dinometer (PDC01, Everte Inc., China). The mean elevations and slopes of the three slope positions are shown in Table 1.

Three plots sized 2 m×5 m were created for measurements of surface runoff and centered at locations 6, 18 and 30, which were representatives of the upper, middle, and lower slope positions (Fig. 1b). Surface runoff was measured for each rainfall event that produced runoff in 2015 and 2016. Three D20 evaporation pans (diameter, 20 cm; height, 10 cm) with 5-cm mesh-wire screen covers were installed next to the runoff monitoring plots at the upper, middle, and lower slope positions. The D20 pan was placed on a frame 70 cm above the ground and had a 5-cm mesh-wire screen cover to prevent birds from drinking from the pan. Pan evaporation was measured every three days during the observation periods of 2015 and 2016.

A meteorological station was installed adjacent to the upper slope position to monitor daily solar radiation, air temperature, wind speed, relative humidity, precipitation, and other factors. The distributions of daily rainfall and mean air temperatures in the study site from 2015 to 2016 are shown in Figure 2.

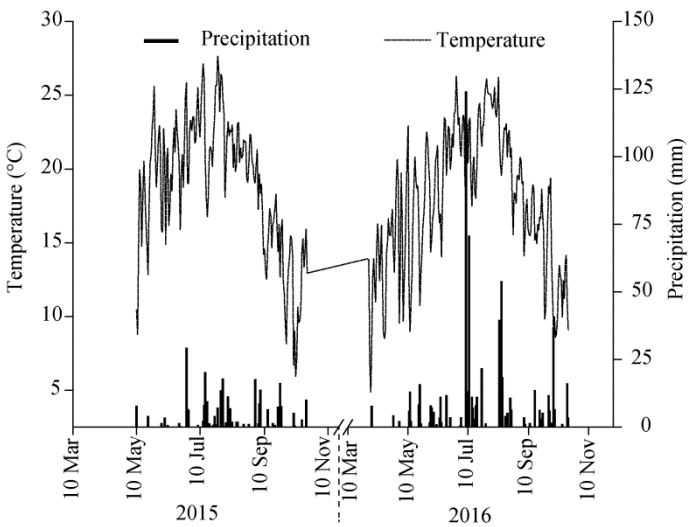

Fig. 2 Distributions of daily precipitation and temperature in the study area during the observation period in 2015 and 2016

2.3 Data analysis

2.3.1 Variation in potential evapotranspiration (PET) along the hillslope

Daily PET was calculated using the Penman equation (Shuttleworth, 1993). The PET calculated by Penman equation in the meteorological monitoring station was regarded as the PET at the upper slope position. Comparisons of PET values were respectively calculated by evaporation pan and Penman equation at the upper slope position on the hillslope (Fig. 3). And the mean ratios of the measured D20 pan evaporation in the upper, middle, and lower slope positions were assumed to be equal to those of PET. Therefore, the ratios of PET in the upper, middle, and lower slope positions were 1.00:0.98:0.83 based on the measurements of D20 pan evaporation.

2.3.2 Actual evapotranspiration (ET_a)

Considering that the temporal interval of soil water measurements along the hillslope was 12 d, the 12-d ET_a (mm/d) was estimated using the water balance method, which was from a reduced equation (Eq. 1).

$$\mathrm{ET_a}_{j+1} = P_{j+1} - R_{j+1} - (\mathrm{SWS}_{j+1} - \mathrm{SWS}_j) - G_{j+1}, \quad (1)$$

where SWS_j is the soil water storage (mm) in the 480-cm profile at the j measurement; SWS_{j+1} is the soil water storage in the 480 cm profile at the j+1 measurement; P_{j+1} is accumulated precipitation (mm) between the j^{th} and j^{th}+1 measurements; R_{j+1} is the accumulated runoff depth between the j and j+1 measurements (mm); and G_{j+1} is deep percolation (mm), which was disregarded because the annual rainfall infiltration depth hardly exceeds 100 cm depth in this area (Yang et al., 2011) and the groundwater table was generally below 20 m in the study site (Shangguan and Zheng, 2006). Precipitation was assumed to be homogenous along the hillslope, whereas the measured runoff depths in the three plots located at the upper, middle, and lower slope positions were assumed valid for the locations 1–13, 14–26, and 27–38, respectively. The underground water was not involved in the soil water cycle due to the high underground water level (Shangguan and Zheng, 2006). Therefore, the influence of groundwater and deep percolation on water balance was disregarded in this study.

2.3.3 Time stability analysis of $\mathrm{ET_a}$

The relative difference method of time stability analysis (Vachaud et al., 1985) was used in this study. The relative difference of $\mathrm{ET_a}$ and δ_{ij} for i location at j time was defined by Equation 2.

$$\delta_{ij} = \frac{\mathrm{ET_a}_{ij} - \overline{\mathrm{ET_a}_j}}{\overline{\mathrm{ET_a}_j}}, \quad (2)$$

where i is the measurement location (i=1, 2, 3,…, n, …, 38); and j is the measurement counting during 2015 and 2016 (j=1, 2, 3, …, m, …, 24). Due to the lack of datasets, hold-out cross-validation method is used to evaluate time stability analysis for estimating the mean $\mathrm{ET_a}$. A random number generator is utilized to randomly select 14 data sets from 24 data sets to form a training set to determine the representative sites. The remaining 10 data sets constitute validation sets, which is to evaluate the prediction accuracy of representative sites for hillslope-mean $\mathrm{ET_a}$. And $\overline{\mathrm{ET_a}_j}$ is the mean $\mathrm{ET_a}$ for all locations at the j measurement and is expressed as Equation 3.

$$\overline{\mathrm{ET_a}_j} = \frac{1}{n}\sum_{i=1}^{n} \mathrm{ET_a}_{ij}, \quad (3)$$

Then, the temporal mean relative difference (MRD), $\overline{\delta}_i$, and its standard deviation (SDRD), or $\sigma(\delta_i)$, were calculated by Equations 4 and 5.

$$\mathrm{MRD} = \frac{1}{m}\sum_{j=i}^{m} \delta_{ij}, \quad (4)$$

$$\mathrm{SDRD} = \sum_{j=1}^{m}\left(\frac{(\delta_{ij} - \overline{\delta}_i)^2}{m-1}\right)^{\frac{1}{2}}. \quad (5)$$

Generally, sampling locations that have relatively low SDRD can be regarded as the locations with high time stability (Grayson and Western, 1998). If the MRD values of sampling locations are close to zero, the $\mathrm{ET_a}$ values in these locations would be close to the area-mean $\mathrm{ET_a}$. Jacobs et al. (2004) suggested an index of time stability (ITS) considering MRD and its SDRD to determine time-stable locations (Eq. 6).

$$\mathrm{ITS}_{ij} = \sqrt{\sigma(\delta_i)^2 + \overline{\delta}_i^{\,2}}. \quad (6)$$

The location with the lowest ITS value was regarded as the MTSL representative of the mean value in $\mathrm{ET_a}$ on the hillslope.

2.3.4 Statistical analysis

The significance level of correlation was tested through a two-tailed t-test. The relationships between $\mathrm{ET_a}$ in each sampling location and the influencing factors were characterized by a non-parametric Spearman's test. The differences of soil properties at different slope positions

were tested through one-way analysis of variance. Tukey's honest significance difference (HSD) method was used as a post hoc test for multiple mean comparisons. K-S (Kolmogorov-Smirnov) test was used to evaluate the normal and non-normal distributions of the time series of SWC. All statistical programs were from SPSS 19.0 (IBM Corp., USA).

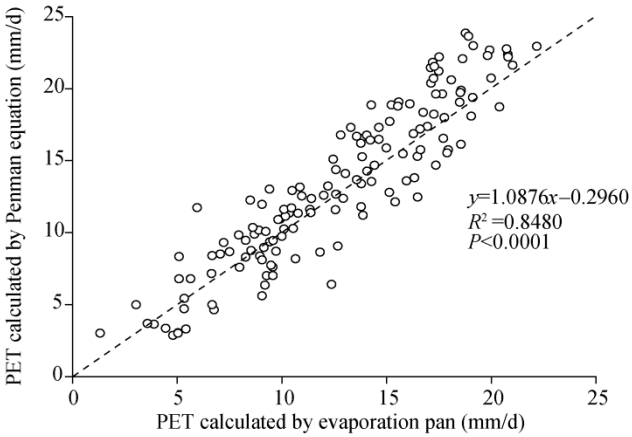

Fig. 3 Comparisons of potential evapotranspiration (PET) values respectively calculated by evaporation pan and penman equation at the upper slope position on the hillslope

3 Results

3.1 Variations in PET and surface runoff at different slope positions

Figure 4 shows the variations in PET at different slope positions during the normal (2015) and wet (2016) water years. The mean values of PET at the upper and middle slope positions were significantly higher (P<0.05) than that at the lower slope position both in 2015 and 2016. PET in the wet water year was higher (P=0.08) than that in the normal water year for all slope positions. Comparisons of runoff between the three slope positions are presented in Figure 5. Only 12 surface runoff events occurred on the hillslope in 2015 and 2016. The mean values exhibited a declining trend from the upper (6.1 mm/d) and middle (3.9 mm/d) to the lower (1.9 mm/d) slope positions. Significant difference was observed only between the upper and lower slope positions (P<0.05).

3.2 Variations in SWC along the hillslope

Normal and non-normal distributions of the time series of SWC were observed at each depth for all locations by a K-S test. Therefore, median and interquartile ranges were used to characterize the central and discrete tendency of SWC during the normal and wet water years (Fig. 6). Areas with the highest SWCs during the normal water year mainly occurred in the 240–480 cm soil layer at the locations of 13, 14, 15, 33, 34, 35 and 36 (Fig. 6a). The other areas with the highest SWCs were the 30–180 cm soil layer for all locations in 2016 because of the approximately doubled precipitation in 2016 compared with 2015 (Fig. 6b). In 2015, the areas with the lowest SWCs were within the 30–180 cm soil layer for the most of measurement locations (Fig. 6a). In 2016, the driest soil layer typically occurred at the soil surface (0–20 cm) (Fig. 6b).

The temporal variability in SWC was characterized by the interquartile range (Fig. 6c and d) for 2015 and 2016. In 2015, the highest temporal variability in SWC was observed in the 0–30 cm soil layer for all locations and in the 40–480 cm soil layer for the locations 13 and 14 (Fig. 6c), whereas, in 2016, the highest temporal stability of SWC extended to the 200 cm depth (Fig. 6d). During the transition from dry to wet period, the SWCs of the 200–480 cm soil layer also remained relatively constant (Fig. 6c and d).

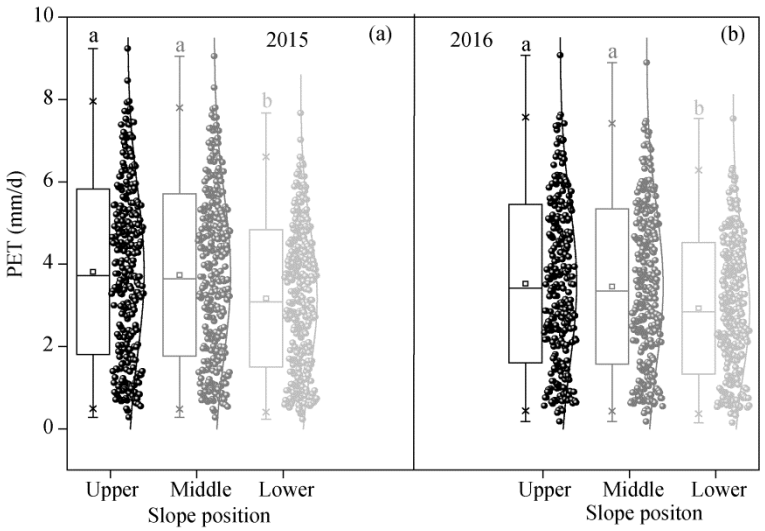

Fig. 4 Daily potential evapotranspiration (PET) at the upper, middle, and lower slope positions during the normal (2015, a) and wet (2016, b) water years. Vertical bars represent standard deviations, the same lowercase letters labelled over the boxes indicate no significant difference at $P<0.05$ level.

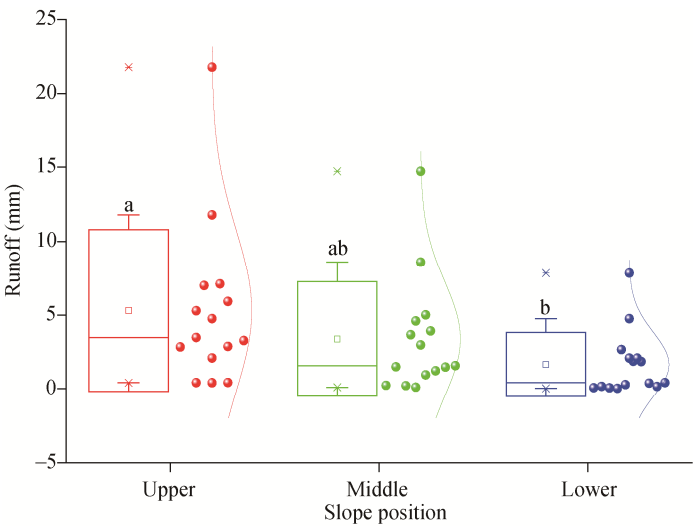

Fig. 5 Variations in surface runoff depth at different slope positions in 2015 and 2016. Vertical bars represent standard deviations, the same lowercase letters labelled over the boxes indicate no significant difference at $P<0.05$ level.

3.3 Variations in ET_a along the hillslope

Figure 7 presents the ET_a in each measurement location along the hillslope during the growing seasons of 2015 and 2016. Despite the different absolute values, the ET_a along the hillslope exhibited a similar trend during normal and wet water years (Fig. 7). ET_a rapidly decreased between locations 1 and 11 to reach the minimum of 226 mm in 2015 and 522 mm in 2016 in location 11 (Fig. 7). Then, ET_a increased and reached the maximum of 291 mm in location 13 in 2015 and 687 mm in location 15 in 2016 (Fig. 7). After reaching the peak, ET_a gradually decreased. ET_a decreases of 41 and 177 mm in 2015 and 2016, respectively, were observed. The mean ET_a in the lower slope positions (locations 27 to 38) was lower than that at the middle slope positions (locations 13 to 26) in the normal and wet years. Furthermore, the ET_a on the hillslope in 2016 was significantly ($P<0.01$) higher than that in 2015, with averaged values of 593 and 270 mm, respectively, due to different amounts of precipitation.

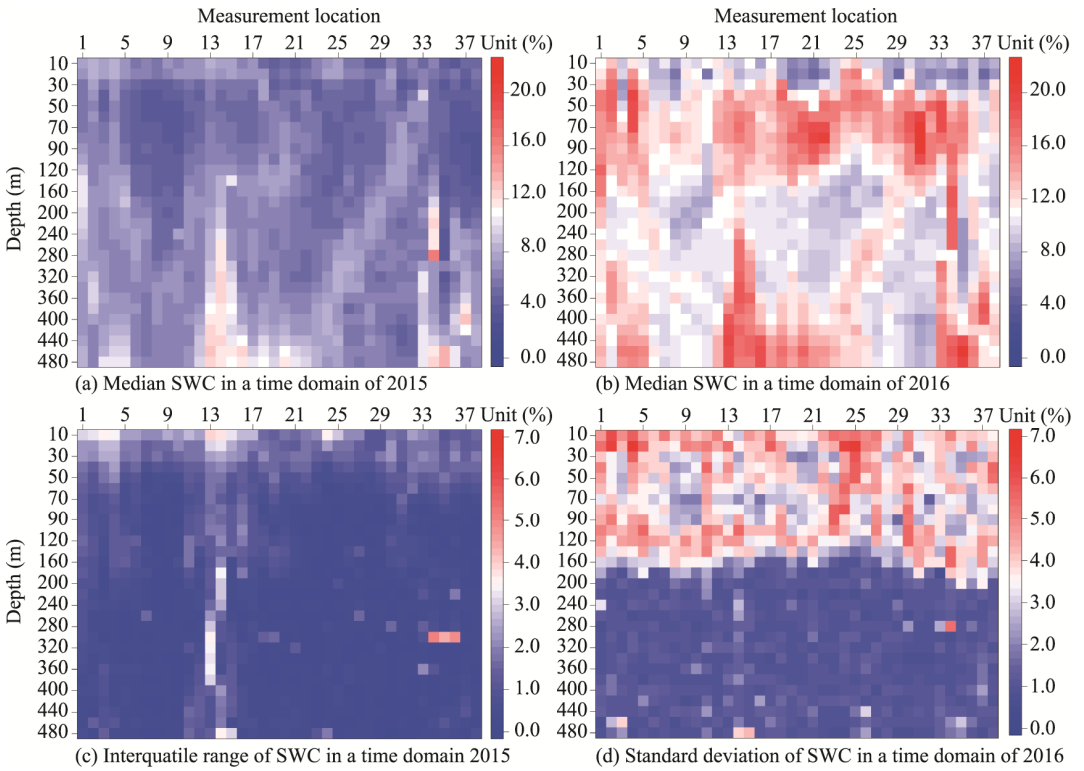

Fig. 6 Median and interquartile ranges of soil water content (SWC) in the time domains of 2015 (a and c) and 2016 (b and d) for various depths and sampling locations

3.4 Time stability of ET_a

A relative difference analysis was performed to quantitatively identify the location where ET_a was consistently equal to the mean ET_a of the study area. Such location identified could approximately represent the area-averaged value of the ET_a, therefore reducing the time, labor and costs for monitoring ET_a. Figure 8 presents the ranked MRD in ET_a, the associated SDRD and the ITS for each sampling location on the hillslope. The mean, minimum, maximum and range values of MRD, SDRD and ITS of ET_a are displayed in Table 2. The ranges (differences between the minimum and maximum values) of MRD, SDRD and ITS were 64.04%, 91.96% and 99.22%, respectively (Table 2). The minimum values of MRD, SDRD and ITS in ET_a were −20.92%, 21.44% and 22.10%, respectively. A significantly positive correlation (P<0.01) was found between MRD and SDRD values in ET_a. In this study, the MTSL with the lowest ITS value was selected to estimate the mean ET_a of the hillslope. As shown in Figure 8, location 13 with an ITS value of 22.10% was identified for estimation of hillslope mean ET_a. The validation dataset verified that the ET_a at the MTSL (location 13) can be used to predict the mean ET_a of the hillslope (R^2=0.931, P<0.01; Fig. 9).

Table 2 Descriptive statistics of MRD, SDRD, and ITS values in ET_a in each sampling location along the hillslope

Parameter	Maximum	Minimum	Mean	SD	Kurtosis	Skewness
MRD (%)	43.12	–20.92	0.00	15.86	1.373	1.265
SDRD (%)	113.40	21.44	42.10	20.24	5.061	2.131
ITS (%)	121.32	22.10	44.32	21.54	5.738	2.287

Note: MRD, mean relative difference; SDRD, standard deviation of relative difference; ITS, index of time stability; ET_a, actual evapotranspiration; SD, standard deviation.

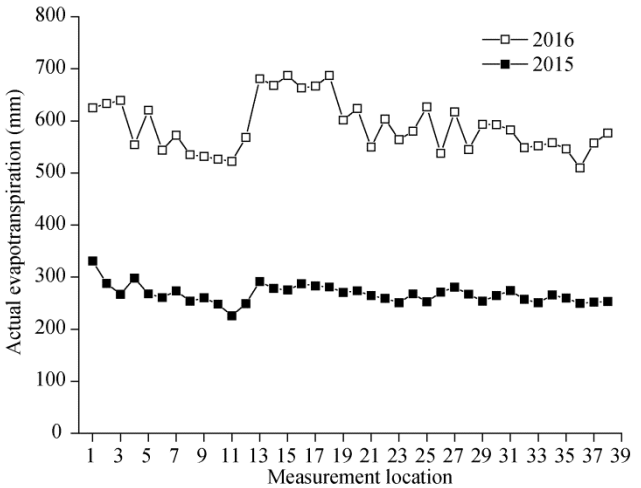

Fig. 7 Variations in accumulated actual evapotranspiration (ET_a) in each sampling location along the hillslope during normal (2015) and wet (2016) water years

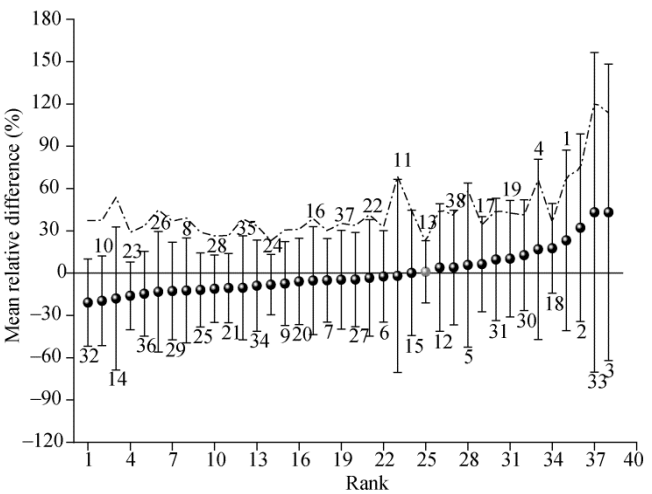

Fig. 8 Ranked mean relative difference (MRD) of actual evapotranspiration (ET_a) and the index of time stability (ITS) for each monitoring location on the hillslope. Vertical bars represent ±1 standard deviation of relative difference (SDRD). The dashed curve indicates ITS, and the most time stable location (MTSL) with the lowest ITS values is marked in grey.

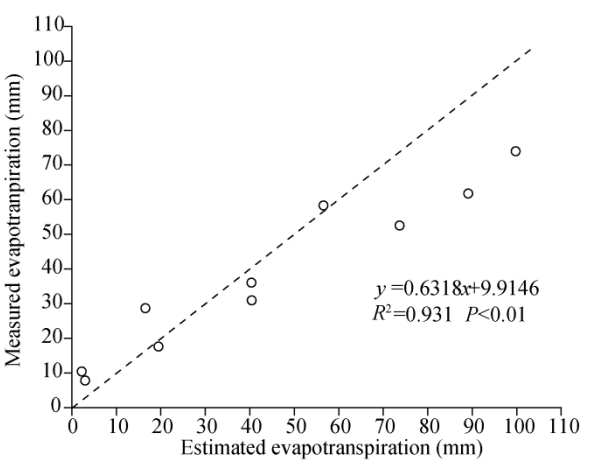

Fig. 9 Predicted versus measured ET_a on the hillslope. The dashed line is the 1:1 line.

3.5 Factors controlling the time stability of ET_a

Table 3 presents the correlations between indices (MRD, SDRD and ITS) exhibiting time stability of ET_a and the factors, i.e., clay contents, K_s, BD, elevation, maximum LAI (LAI_m) and SWS. The MRD of ET_a is another manifestation of evapotranspiration size. As shown in Table 3, MRD values of ET_a had the highest positive correlation with SWS (P<0.01); besides, ELE and PCC (mean clay contents for the profile) was also correlated with MRD of ET_a (P<0.05). SDRD and ITS values in this study represent the time stability of ET_a. According to Table 3, only ELE was significantly correlated with SDRD and ITS values of ET_a (P<0.05).

Among the influencing factors, LAI_m and BD were positively correlated (P<0.01). ELE had a significant relationship with LAI_m, BD and SCC (surface clay contents) (P<0.01). The SCC was negatively correlated with BD (P<0.01). In addition, a significantly positive correlation existed between SWS and PCC (P<0.05). A relatively weak correlation, however, was presented between MRD of ET_a and LAI_m (P>0.05).

Table 3 Matrix of Spearman rank correlation coefficients for factors influencing the mean relative difference (MRD), standard deviation of relative difference (SDRD) and index of time stability (ITS) of actual evapotranspiration (ET_a)

	MRD	SDRD	ITS	BD	K_s	ELE	LAI_m	SWS	SCC	PMCC
MRD	1.000									
SDRD	0.787**	1.000								
ITS	0.784**	0.996**	1.000							
BD	0.066	–0.055	–0.041	1.000						
K_s	0.240	0.324*	0.308	0.187	1.000					
ELE	0.375*	0.335*	0.331*	–0.543**	0.007	1.000				
LAI_m	–0.306	–0.309	–0.308	0.426**	0.191	–0.698**	1.000			
SWS	0.504**	0.316	0.312	0.029	0.165	0.150	–0.099	1.000		
SCC	0.140	0.022	0.032	–0.502**	–0.057	0.466**	–0.316	0.265	1.000	
PMCC	0.322*	0.015	0.011	0.239	0.328*	–0.070	0.081	0.370*	0.217	1.000

Note: MRD, SDRD and ITS indicate mean relative difference (MRD), standard deviation of relative difference (SDRD) and index of time stability (ITS) of actual evapotranspiration (ET_a). SCC, surface clay contents; PMCC, profile mean clay contents; SWS, soil water storage; * and ** indicate that the correlation is significant at P<0.05 and P<0.01 levels, respectively.

Table 4 Matrix of Spearman rank correlation coefficients between potential evapotranspiration (PET) and five climatic factors

Parameter		T_{max} (°C)	T_{min} (°C)	Rs (MJ/m^2)	Ws (m/s)	Td (°C)
PET	Pearson correlation	0.816**	0.700**	0.890**	0.185**	0.429**
	Sig. (2-tailed)	0.000	0.000	0.000	0.000	0.000
	N	1025	1025	1025	1025	1025

Note: Sig., significant level; *N*, sample size; T_{max}, maximum temperature; T_{min}, minimum temperature; Rs, solar radiation; Ws, wind speed; Td, dewpoint temperature. ** indicates that the correlation is significant at P<0.01 level.

4 Discussion

4.1 Variations of components in water balance along the hillslope

PET was influenced by climatic conditions, such as solar radiation, air temperature, wind speed and relative humidity, which can be used to estimate ET_a in the water balance calculations. Given that one of the important environmental controls in PET is solar radiation (Table 4), the small PET in the lower slope position (Fig. 4) might be due to reduced solar radiation (Carey and Woo, 2011; Fyllas et al., 2017). The precipitation in 2016 was much more than that in 2015; however, PET in both years did not show a significant difference (Fig. 4). The results indicated that PET exhibited less inter-annual variability than precipitation in the studied area. This observation was consistent with that in the study of Oishi et al. (2010), who studied the evapotranspiration of a mature oak-hickory forest in North Carolina of USA and found that despite the large inter-annual

variation in precipitation (ranging from 934 to 1346 mm), annual evapotranspiration varied much less (610–668 mm). This was because inter-annual evapotranspiration variability can be mitigated by vegetation responses through decreasing soil water storage during drought period (Jones, 2011).

Surface runoff is affected by many factors, such as rainfall intensity, rainfall duration, presence of vegetation, soil and microtopography (Dunne et al., 1991; El-Hassanin et al., 1993). Surface runoff decreased gradually from upper to lower slope position (Fig. 5). Given that rainfall was consistent across the hillslope, variations in surface runoff could be mainly attributed to the difference in the slope gradient (Table 1)**.** This conclusion was also supported by El-Hassanin et al. (1993), who reported that runoff increased as the slope gradient increased. The median values of runoff for the three slope positions were as small as 3.5 mm/d, and only 12 runoff events occurred during the two years. These results indicated that in the semi-arid area, the amount and frequency of runoff events was so limited that it had little influence on the water balance calculations.

Larger water storage was concentrated in the deep soil layer (i.e., 240–480 cm) of the lower slope position (Fig. 6a and b). A similar observation was obtained by Fu et al. (2013), who reported that soil water downhill accumulation occurred in a deep soil layer (i.e., 300–400 cm) for fallow and cropland due to elevation. Due to rapidly increased precipitation, spatial pattern of SWC in the vertical profile has significantly changed from 2015 to 2016 (Fig. 6). For instance, the 30–180 cm soil layer of the hillslope was the driest layer in 2015. This is because this layer was the main distribution area of the root system of *C. korshinskii* (Cheng et al., 2009), and became the driest soil layer for the root water uptake. Then, the 30–180 cm soil layer was converted to the wettest areas because of the doubled precipitation in 2016 compared with 2015 (Fig. 6b). This result agreed with the findings of Chen et al. (2008), who observed that stored water in grassland in the 200–300 cm soil layer greatly increased due to doubled precipitation in the Chinese Loess Plateau. The highest temporal variability of SWC in 2015 and 2016 was observed in 0–30 and 0–200 cm soil layer, respectively (Fig. 6c and d). The former was due to the combined effects of precipitation, solar radiation, soil evaporation and topography on the surface soil layer (i.e., 0–30 cm soil layer in this study) (Wythers et al., 1999; Pan and Wang, 2009; Gao et al., 2015); the latter was probably a result of precipitation recharge to root zone SWC, which resulted in the transition from driest to wettest in the root zone.

ET_a varied with terrain, climate, soil, and plant characteristics. ET_a in this study exhibited a slightly declining trend (Fig. 7). Based on the simplified water balance on the studied hillslope (not considering rainfall, deep percolation and groundwater recharge (Shangguan and Zheng, 2006; Yang et al., 2011)), variations of ET_a were mainly ascribed to variations of SWS and surface runoff. For SWS, no significant difference was found for temporal variability (displayed by interquartile range) of SWC among sampling sites along the hillslope (Fig. 6c and d), indicating that variation degrees of water storage for all measurement sites were similar. Therefore, the slightly declining trend in ET_a along the hillslope mainly resulted from variations of surface runoff (Fig. 5). Besides, the significantly low PET (P<0.05) at the lower slope position (Fig. 4) also supported the declining trend in ET_a on the hillslope in this study. ET_a along the hillslope exhibited a similar trend during the normal and wet water years (Fig. 7). This indicated that the horizontal spatial pattern of ET_a on the hillslope was hardly altered by precipitation in semi-arid areas. The reason was that, based on the simplified water balance, ET_a was mainly affected by variations of SWS and surface runoff depth. For the former, the horizontal spatial pattern of SWS on the hillslope changed little because the increased SWS in the semi-arid areas typically resulted in water flow in the vertical profile by soil properties (Grayson et al., 1997; Green and Erskine, 2011). For the latter, horizontal overland flow could indeed influence soil water horizontal distribution. However, the amount and frequency of runoff were quite limited in this study (Fig. 5). Among locations 1–17 (Fig. 7), location 11 had almost the lowest ET_a in both 2015 and 2016. Location 11 also had the lowest SWC of the whole hillslope (Fig. 6). The reason for the low ET_a in location 11 might be that low SWC limited the plant growth in semi-arid areas (Linacre, 2004), and resulted in lower water consumption by transpiration. ET_a around location

14 was higher than that in most of the hillslope (Fig. 7). High ET_a around location 14 could be ascribed to the high water storage in this area (Fig. 6a and b). This was because that increased water storage in arid and semi-arid areas could greatly promote plant growth, thus leading to high ET_a (Garcia and Tague, 2014).

4.2 Time stability of ET_a and its influencing factors

Time stability has been substantially applied to SWC in previous studies (Vachaud et al., 1985; Jacobs et al., 2004; Gao and Shao, 2012; Zhang et al., 2016). In addition to SWC, time stability, as an effective method to analyze spatiotemporal variability, was first applied to soil sulfur content and soil salinity (Douaik et al., 2006; Piotrowska-Długosz et al., 2017). In this study, a time stability analysis was performed to investigate the spatiotemporal variability of ET_a for the first time. The ranges of SDRD and ITS in ET_a were 145.38 and 151.42 (Table 2), which were significantly higher than those in SWC (Gao and Shao, 2012; Zhang et al., 2016). The phenomenon indicated that ET_a had a relatively higher temporal variability than SWC. It was because that the components (soil evaporation and transpiration) of ET_a and the corresponding controls in the components were so numerous and the variability of ET_a was greatly increased (Zeng and Cai, 2016). The minimum SDRD and ITS in ET_a were not significantly higher than those in SWC (Table 2). The results indicated that the location with the lowest ITS values could be used to accurately estimate the hillslope mean ET_a. The MRD and SDRD values in ET_a at each measurement location had a significantly positive relationship (P<0.01). The correlation suggested that a high ET_a (presented as high MRD) would cause high temporal variability of ET_a (presented as high SDRD). A similar observation was obtained by Vivoni et al. (2010), who investigated the spatiotemporal variability of soil moisture and evapotranspiration in a mountainous basin within the North American monsoon region. This finding also indicated that the location with high time stability in ET_a (presented as low SDRD) tended to be in the area with relatively low ET_a (presented as low MRD) along the hillslope. Figure 8 shows that MTSL (location 13) could be used to estimate the hillslope mean ET_a (R^2=0.931, P<0.01), which could be estimated with MTSL identified from the time stability analysis. In the future monitoring process, the ET_a value at the MTSL can be continuously monitored by an automatic device, and can represent the average ET_a of the whole hillslope. This method will also save a great deal of labor, time and expenditure.

ET_a involves soil evaporation and plant transpiration through the stomata of plants, and is influenced by hydrological processes, such as precipitation, runoff and underground water. Therefore, the time stability of ET_a was directly or indirectly affected by terrain, soil, climate and vegetation characteristics. MRD of ET_a can represent the ET_a size. In this study, a significantly positive relationship (P<0.01) existed between SWS and MRD of ET_a (Table 3). With regard to this point, Manabe (1969) proposed two SWC thresholds, namely, SWC_{CRIT} (critical water content above which ET_a equals PET) and SWC_{WILT} (soil wilting coefficient below which ET_a is zero), and suggested that ET_a increased with increasing SWC between the two SWC thresholds. Shuttleworth (1993) found that SWC_{CRIT} was typically equal to 50%–80% of SWC_{FC} (field capacity). In this study, most of SWCs were within these two thresholds. The positive relationship between ET_a and SWS (P<0.05) also supported the conclusion of Manabe (1969), who considered ET_a increased with the increasing SWC, as SWC values were between SWC_{CRIT} and SWC_{WILT}. Similar observations were also obtained in other studies (Vivoni et al., 2010; Garcia and Tague, 2014). Furthermore, a significantly positive relationship existed among MRD of ET_a, SWS and PMCC (profile mean clay contents) (Table 3). Thus, it can be inferred that soil texture influenced the SWS distribution and resulted in the spatial variability of ET_a because soil texture controlled the vertical water distribution in the profile (Grayson et al., 1997). Moreover, lateral overland flow was so infrequent (Fig. 4) that horizontal soil water redistribution seldom occurred. Besides, only ELE had significant correlation with SDRD and ITS of ET_a (Table 3) because ELE could affect the time stability of ET_a by indirectly influencing soil and vegetation on a hillslope. This was also supported by Table 3, which displayed that ELE was negatively correlated with BD and LAI but positively correlated with SCC (P<0.01). A weak correlation existed between LAI_m and ET_a (Table 3)

because considerable areas of bare soil between shrubs during the growing season causing high evaporation. Soil evaporation, however, was not associated with plant productivity compared with plant transpiration (Kool et al., 2014) and eventually weakened the positive correlation between ET_a and LAI_m.

5 Conclusions

In this study, soil water storage, surface runoff and precipitation along a hillslope were determined during the normal (2015) and wet (2016) water years. ET_a was calculated from a simple water balance equation. The spatial variability and time stability of ET_a along the hillslope were investigated, and the key factors that influence the spatiotemporal variability of ET_a were analyzed. The conclusions were obtained as follow: (1) lower slope position showed less potential evapotranspiration probably due to reduced solar radiation compared with the upper and middle slope positions; (2) horizontal spatial pattern of ET_a on the hillslope was hardly altered by precipitation in semi-arid areas although doubled precipitation increased ET_a; (3) time stability analysis indicated that the location with high time stability of ET_a tended to be in the area with relatively low ET_a. The location with the highest time stability of ET_a can be used to accurately estimate the mean ET_a of the hillslope; and (4) time stability of ET_a was mainly ascribed to elevation on the hillslope of Chinese Loess Plateau.

Acknowledgements

This research was financially supported by the Programme of Introducing Talents of Discipline to Universities of China (D18013), the independent subject of State Key Laboratory of Plateau Ecology and Agriculture, Qinghai University, China (2019-ZZ-05), the Project of Qinghai Science & Technology Department (2019-ZJ-Y01), the Natural Science Foundation of Qinghai Province, China (2020-ZJ-967Q), the Thousand High Innovative Talents Program of Qinghai Province (2019), and the Program for Changjiang Scholars and Innovative Research Team in University, Ministry of Education, China (IRT_17R62). The authors would also like to thank the staff of Shenmu Erosion and Environment Station of the Institute of Soil and Water Conservation, Chinese Academy of Sciences.

References

Baker J M. 1990. Measurement of soil water content. Remote Sensing Reviews, 5(1): 263–279.

Bo X, Wang Q H, Fan J, et al. 2011. Application of the SCS-CN model to runoff estimation in a small watershed with high spatial heterogeneity. Pedosphere, 21(6): 738–749.

Bromley J, Brouwer J, Barker A, et al. 1997. The role of surface water redistribution in an area of patterned vegetation in a semi-arid environment, south-west Niger. Journal of Hydrology, 198(1–4): 1–29.

Carey S K, Woo M. 2001. Spatial variability of hillslope water balance, wolf creek basin, subarctic yukon. Hydrological Process, 15(16): 3113–3132.

Chen H S, Shao M G, Li Y Y. 2008. The characteristics of soil water cycle and water balance on steep grassland under natural and simulated rainfall conditions in the Loess Plateau of China. Journal of Hydrology, 360(1–4): 242–251.

Cheng X R, Huang M B, Shao M G, et al. 2009. A comparison of fine root distribution and water consumption of mature Caragana korshinkii Kom grown in two soils in a semiarid region, China. Plant and Soil, 315(1–2): 149–161.

Douaik A, van Meirvenne M, Toth T. 2006. Temporal stability of spatial patterns of soil salinity determined from laboratory and field electrolytic conductivity. Arid Land Research and Management, 20(1): 1–13.

Dunne T, Zhang W, Aubry B F. 1991. Effects of rainfall, vegetation, and microtopography on infiltration and runoff. Water Resources Research, 27(9): 2271–2285.

El-Hassanin A S, Labib T M, Gaber E I. 1993. Effect of vegetation cover and land slope on runoff and soil losses from the watersheds of Burundi. Agriculture Ecosystems & Environment, 43(3–4): 301–308.

Ewers B E, Mackay D S, Gower S T, et al. 2002. Tree species effects on stand transpiration in northern Wisconsin. Water Resources Research, 38(7): 1103, doi: 10.1029/2011WR010636.

Fu W, Huang M B, Gallichand J, et al. 2012. Optimization of plant coverage in relation to water balance in the Loess Plateau of China. Geoderma, 173–174: 134–144.

Fu X L, Shao M G, Wei X R, et al. 2013. Effects of monovegetation restoration types on soil water distribution and balance on a

hillslope in northern loess plateau of China. Journal of Hydrologic Engineering, 18(4): 413–421.

Fyllas N M, Bentley L P, Shenkin A, et al. 2017. Solar radiation and functional traits explain the decline of forest primary productivity along a tropical elevation gradient. Ecology Letters, 20(6): 730–740.

Gao G, Chen D L, Xu C Y, et al. 2007. Trend of estimated actual evapotranspiration over China during 1960–2002. Journal of Geophysical Research-Atmospheres, 112: D11120, doi: 10.1029/ 2006JD008010.

Gao L, Shao M. 2012. Temporal stability of shallow soil water content for three adjacent transects on a hillslope. Agricultural Water Management, 110: 41–54.

Gao L, Lv Y J, Wang D D, et al. 2015. Can shallow-layer measurements at a single location be used to predict deep soil water storage at the slope scale? Journal of Hydrology, 531: 534–542.

Gao X D, Wu P T, Zhao X N, et al. 2011. Estimating spatial mean soil water contents of sloping jujube orchards using temporal stability. Agricultural Water Management, 102(1): 66–73.

Gao Y F, Zhao C Y, Muhammad W A, et al. 2019. Actual evapotranspiration of subalpine meadows in the Qilian Mountains, Northwest China. Journal of Arid Land, 11(3): 371–384.

Garcia E, Tague C. 2014. Climate regime and soil storage capacity interact to effect evapotranspiration in western United States mountain catchments. Hydrology And Earth System Sciences, 11(2): 2277–2319.

Gardner C M K, Robinson D, Blyth K, et al. 2001. Soil water content. In: Smith K A, Mullins C E. Soil and Environmental Analysis: Physical methods (2nd ed.). New York: Marcel Dekker, 1–64.

Grayson R B, Western A W, Chiew F H, et al. 1997. Preferred states in spatial soil moisture patterns: Local and nonlocal controls. Water Resources Research, 33(12): 2897–2908.

Grayson R B, Western A W. 1998. Towards areal estimation of soil water content from point measurements: time and space stability of mean response. Journal of Hydrology, 207(1–2): 68–82.

Green T R, Erskine R H. 2011. Measurement and inference of profile soil-water dynamics at different hillslope positions in a semiarid agricultural watershed. Water Resources Research, 47(12): W00H15, doi: 10.1029/2010WR010074.

Hu W, Shao, M A, Han F, et al. 2010. Watershed scale temporal stability of soil water content. Geoderma, 158(3–4): 181–198.

Hu W, Si B C. 2014. Can soil water measurements at a certain depth be used to estimate mean soil water content of a soil profile at a point or at a hillslope scale? Journal of Hydrology, 516: 67–75.

Jacobs J M, Mohanty B P, Hsu E C, et al. 2004. SMEX02: Field scale variability, time stability and similarity of soil moisture. Remote Sensing of Environment, 92(4): 436–446.

Jia Y H, Shao M A. 2013. Temporal stability of soil water storage under four types of revegetation on the northern Loess Plateau of China. Agricultural Water Management, 117: 33–42.

Jones J. 2011. Hydrologic responses to climate change: Considering geographic context and alternative hypotheses. Hydrological Process, 25(12): 1996–2000.

Kool D, Agam N, Lazarovitch N, et al. 2014. A review of approaches for evapotranspiration partitioning. Agricultural and Forest Meteorology, 184: 56–70.

Li Q Y, Sun Y W, Yuan W L, et al. 2017. Streamflow responses to climate change and LUCC in a semi-arid watershed of Chinese Loess Plateau. Journal of Arid Land, 9(4): 609–621.

Lian J, Huang M. 2015. Evapotranspiration estimation for an oasis area in the Heihe River Basin using Landsat-8 images and the METRIC model. Water Resources Management, 29(14): 51–57.

Lian J, Huang M. 2016. Comparison of three remote sensing based models to estimate evapotranspiration in an oasis-desert region. Agricultural Water Management, 165: 153–162.

Liao K, Zhou Z, Lai X, et al. 2017. Evaluation of different approaches for identifying optimal sites to predict mean hillslope soil moisture content. Journal of Hydrology, 547: 10–20.

Libardi P L, Reichardt K, Nielsen D R, et al. 1980. Simple field methods for estimating soil hydraulic conductivity. Soil Science Society of America Journal, 44(1): 3–7.

Linacre E. 2004. Evaporation trends. Theoretical and Applied Climatology, 79: 11–21.

Majidi M, Alizadeh A, Vazifedoust M, et al. 2015. Analysis of the effect of missing weather data on estimating daily reference evapotranspiration under different climatic conditions. Water Resources Management, 29(7): 2107–2124.

Manabe S. 1969. Climate and the ocean circulation: I. The atmospheric circulation and the hydrology of the earth's surface. Monthly Weather Review, 97(11): 739–774.

McVicar T R, van Niel T G, Li L T, et al. 2007. Spatially distributing monthly reference evapotranspiration and pan evaporation considering topographic influences. Journal of Hydrology, 338(3–4): 196–220.

Mitchell P J, Benyon R G, Lane P N. 2012. Responses of evapotranspiration at different topographic positions and catchment water balance following a pronounced drought in a mixed species eucalypt forest, Australia. Journal of Hydrology, 440–441:

62–74.

Mo X G, Liu S X, Lin Z H, et al. 2004. Simulating temporal and spatial variation of evapotranspiration over the Lushi basin. Journal of Hydrology, 285(1–4): 125–142.

Newman B D, Wilcox B P, Archer S R, et al. 2006. Ecohydrology of water-limited environments: A scientific vision. Water Resources Research, 42(6): W06302, doi: 10.1029/ 2005WR004141.

Nicholls E M, Carey S K, Humphreys E R, et al. 2016. Multi-year water balance assessment of a newly constructed wetland, Fort McMurray, Alberta. Hydrological Processes, 30(16): 2739–2753.

Oishi A C R, Oren K A, Novick S, et al. 2010. Interannual invariability of forest evapotranspiration and its consequence to water flow downstream. Ecosystems, 13: 421–436.

Pan Y X, Wang X P. 2009. Factors controlling the spatial variability of surface soil moisture within revegetated-stabilized desert ecosystems of the Tengger Desert, Northern China. Hydrological Process, 23(11): 1591–1601.

Peel M C, Finlayson B L, McMahon T A. 2007. Updated world map of the Köppen-Geiger climate classification. Hydrology and Earth System Sciences Discussions, 4(2): 439–473.

Piotrowska-Długosz A, Siwik-Ziomek A, Długosz J, et al. 2017. Spatio-temporal variability of soil sulfur content and arylsulfatase activity at a conventionally managed arable field. Geoderma, 295: 107–118.

Santiago L S, Goldstein G, Meinzer F C, et al. 2000. Transpiration and forest structure in relation to soil waterlogging in a Hawaiian montane cloud forest. Tree Physiology, 20(10): 673–681.

Shangguan Z P, Zheng S X. 2006. Ecological properties of soil water and effects on forest vegetation in the Loess Plateau. International Journal of Sustainable Development & World Ecology, 13(4): 307–314.

Shuttleworth W J. 1993. Evaporation. In: Maidment D R. Handbook of Hydrology. Sydney: McGraw-Hill.

Starr G. 2005. Assessing temporal stability and spatial variability of soil water patterns with implications for precision water management. Agricultural Water Management, 72(3): 223–243.

Thomas A. 2000. Spatial and temporal characteristics of potential evapotranspiration trends over China. International Journal of Climatology, 20(4): 381–396.

Vachaud G, Passerat de Silans A, Balabanis P, et al. 1985. Temporal stability of spatially measured soil water probability density function. Soil Science Society of America Journal, 49(4): 822–828.

Vivoni E R, Rodriguez J C, Watts C J. 2010. On the spatiotemporal variability of soil moisture and evapotranspiration in a mountainous basin within the North American monsoon region. Water Resources Research, 46(2): W02509, doi: 10.1029/2009WR008240.

Wilcox B P, Breshears D D, Seyfried M S. 2003. Water balance on rangelands. In: Stewart B A, Howell T A. Encyclopedia of Water Science. New York: Marcel Dekker, Inc., 791–794.

Wythers K R, Lauenroth W K, Paruelo J M. 1999. Bare-soil evaporation under semiarid field conditions. Soil Science Society of America Journal, 63(5): 1341–1349.

Xu C Y, Singh V P. 2005. Evaluation of three complementary relationship evapotranspiration models by water balance approach to estimate actual regional evapotranspiration in different climatic regions. Journal of Hydrology, 308(1–4): 105–121.

Yang L, Wei W, Mo B, et al. 2011. Soil water deficit under different artificial vegetation restoration in the semi-arid hilly region of the Loess Plateau. Acta Ecologica Sinica, 31: 3060–3068. (in Chinese)

Zeng R J, Cai X M. 2016. Climatic and terrestrial storage control on evapotranspiration temporal variability: Analysis of river basins around the world. Geophysical Research Letters, 43(1): 185–195.

Zhang D B, Yao P W, Na Z, et al. 2016. Soil water balance and water use efficiency of dryland wheat in different precipitation years in response to green manure approach. Scientific Reports, 6: 26856, doi: 10.1038/srep26856.

Zhang Y K, Xiao Q L, Huang M B. 2016. Temporal stability analysis identifies soil water relations under different land use types in an oasis agroforestry ecosystem. Geoderma, 271: 150–160.

Zhao L W, Zhao W Z. 2014. Evapotranspiration of an oasis-desert transition zone in the middle stream of Heihe River, Northwest China. Journal of Arid Land, 6(5): 529–539.